Available online at www.sciencedirect.com

ScienceDirect

Geochimica et Cosmochimica Acta 306 (2021) 171–188

Geochimica et Cosmochimica Acta

www.elsevier.com/locate/gca

Anoxic *in situ* production of bacterial GMGTs in the water column and surficial bottom sediments of a meromictic tropical crater lake: Implications for lake paleothermometry

A.J. Baxter [a,*], F. Peterse [a], D. Verschuren [b], J.S. Sinninghe Damsté [a,c]

[a] *Utrecht University, Faculty of Geosciences, Department of Earth Sciences, Princetonlaan 8A, 3584 CB Utrecht, the Netherlands*
[b] *Ghent University, Limnology Unit, K.L. Ledeganckstraat 35, B-9000 Gent, Belgium*
[c] *NIOZ Royal Netherlands Institute for Sea Research, Department of Marine Microbiology and Biogeochemistry, PO Box 59, 1790 AB Den Burg, the Netherlands*

Received 26 October 2020; accepted in revised form 10 May 2021; Available online 19 May 2021

Abstract

Branched glycerol monoalkyl glycerol tetraethers (brGMGTs) are membrane-spanning lipids which were initially identified in marine settings and have more recently been found in peats and lake sediments. In the latter settings, their abundance relative to that of the branched glycerol dialkyl glycerol tetraethers (brGDGTs) appears to increase under warmer climate conditions. Furthermore, their relative distribution in bottom sediments from an altitudinal transect of East African lakes has been linked to local mean annual air temperature (MAAT). To shed light on their sources and identify potential environmental factors driving their production in lakes, we investigated their occurrence and distribution in the water column, surficial lake-bottom sediments, and catchment soils of Lake Chala, a permanently stratified (meromictic) tropical crater lake in East Africa. Data from the water column comprise both suspended particulate matter (SPM) collected monthly at eight depth intervals between 0 and 80 m for 17 consecutive months, and settling particles collected monthly at a depth of 35 m over a period of 53 months. In catchment soils, brGMGTs are either relatively scarce or absent. In the water column, their occurrence is dominated by four of the seven known brGMGTs and mostly limited to the anoxic zone. Whereas the spatial distribution and concentration of brGMGTs in SPM were strongly influenced by the seasonal cycle of strong water-column stratification alternating with deep mixing, this trend is not consistent on the multi-year timescale of the settling-particles record. Moreover, their relative distribution in both SPM and settling particles did not respond to temperature variation during the studied interval. In contrast to the water column, surficial lake-bottom sediments contain the full suite of known brGMGTs in a distinct and spatially uniform fractional abundance, strongly suggesting that the majority of brGMGT production takes place there. BrGMGT-inferred MAAT for the Chala area reasonably estimates measured MAAT and conforms to the East African lake brGMGT calibration. Our results have important implications for the use of brGMGTs as proxy for MAAT, in that outside of the equatorial zone the presumably greater offset between bottom-water temperature and MAAT may create a bias towards cold-season air temperature. Regardless, the more singular source of brGMGTs in lake sediments is an advantage for paleotemperature reconstruction compared to brGDGTs, which several studies now indicate to have a

* Corresponding author.
E-mail address: A.J.Baxter@uu.nl (A.J. Baxter).

https://doi.org/10.1016/j.gca.2021.05.015

mixed aquatic and terrestrial source of which the relative contribution cannot easily be disentangled or assumed to have been constant through time.

Keywords: brGMGTs; H-brGDGTs; East Africa; Lake Chala; *In situ* production

1. INTRODUCTION

In order to answer crucial questions about the development of Earth's climate system within the context of anthropogenic climate change, it is essential to accurately document both global and regional-scale temperature fluctuations throughout Earth's history. As direct measurement of climate-related variables in the past is impossible, this is achieved by the use of paleoclimate proxies, i.e., physical, chemical or biological features which are preserved in the geological record and provide insight into past climatic conditions. Natural archives containing established climate proxies for the Quaternary Period are unevenly distributed around the globe, leading to a particular need for more reliable proxies specifically applicable to continental environments and the tropical regions. Lakes are valuable archives of regional climate variability on the continents. Lake sediments are often high in organic matter content which has been either produced *in situ* or washed into the lake, and therefore they catalogue various processes within the lake and its surroundings that are influenced by climate (Cohen, 2003). Lakes are particularly valuable climate archives in tropical continental regions, where long climate records with high temporal resolution are still scarce (Verschuren et al., 2013; Johnson et al., 2016). Lipid biomarkers preserved in lake sediments, such as plant waxes and microbial membrane lipids, can give insight into past and present environmental change, often with greater specificity than bulk organic proxies (Meyers, 2003; Castañeda and Schouten, 2011; Berke, 2018). Moreover, some lipids behave as quasi thermometers, reacting to temperature in a semi-quantitative way (Powers et al., 2004; Tierney et al., 2010; Pearson et al., 2011; Loomis et al., 2012; 2014; Russell et al., 2018; Baxter et al., 2019).

Glycerol dialkyl glycerol tetraethers (GDGTs) are the basis of several established lipid paleothermometers. The two main groups of interest to paleoclimatologists are generally isoprenoid GDGTs (isoGDGTs) and branched GDGTs (brGDGTs; Fig. 1). IsoGDGTs are produced by several different species of archaea (for a review, see Schouten et al., 2013). In the marine realm, their structural diversity relates to sea surface temperature (Schouten et al., 2002; Kim et al., 2010), and based on their down-core variation in marine sediments, paleotemperature records of varying geological age have now been generated for several world regions (e.g. Sluijs et al., 2006; Castañeda et al., 2010; dos Santos et al., 2010). Based on the stereochemistry of their glycerol moiety, brGDGTs are thought to be produced by bacteria (Weijers et al., 2006a) and are found particularly abundantly in soils (Weijers et al., 2006b, 2007) and peats (Sinninghe Damsté et al., 2000). They vary in the number of their cyclo-pentane moieties (0–2) and in the number (tetra-, penta- or hexamethylated) and position (5th or 6th carbon) of additional methyl groups (Fig. 1; Sinninghe Damsté et al., 2000; Weijers et al., 2006a; De Jonge et al., 2013). Using data from peats and soils worldwide, mean annual air temperature (MAAT) and pH have been identified as the major environmental factors controlling the structural diversity of brGDGTs, with their degree of methylation relating to MAAT whereas their degree of cyclization and the position of the methyl branch is linked to pH (e.g. Weijers et al., 2007; De Jonge et al., 2014; Naafs et al., 2017a; 2017b; Dearing Crampton-Flood et al., 2020).

To date, the actual producers of brGDGTs remain largely unknown. Only a few cultures of Acidobacteria from soil have been found to produce minor amounts of the acyclic tetramethylated brGDGT (Ia; Sinninghe Damsté et al., 2011) although their presumed precursors, *iso*-diabolic acids (Fig. 1), are more widespread in the Acidobacteria phylum (Sinninghe Damsté et al., 2018). Most species of subdivision (SD) 4 of the Acidobacteria contain *iso*-diabolic acid ether bound to a glycerol in larger fractional abundance than *iso*-diabolic acid itself, but this trait appears limited to SD 4 (Sinninghe Damsté et al., 2014). Methylated *iso*-diabolic acid derivatives have been found in SDs 1, 3, 4 and 6, but only SD 4 Acidobacteria produce 5-methyl *iso*-diabolic acid derivatives, whereas species of the other SDs form 6-methyl *iso*-diabolic acids. Therefore, many uncertainties concerning the biological origin of brGDGTs remain and bacteria other than Acidobacteria may also produce brGDGTs in natural settings (Chen et al., 2018; Sinninghe Damsté et al., 2018; Weber et al., 2018).

The presence of brGDGTs in lake sediments was initially thought to be due to erosion of terrestrial soils into the lake system (Blaga et al., 2009). More recently, considerable evidence for *in situ* production of brGDGTs in lakes, generally in the anoxic lower water column and/or surficial bottom sediments, is complicating the use of temperature calibrations based on the distribution of brGDGTs in soils (Sinninghe Damsté et al., 2009; Tierney and Russell, 2009; Bechtel et al., 2010; Buckles et al., 2014; Colcord et al., 2017; Weber et al., 2015; 2018; Miller et al., 2018; van Bree et al., 2020). The ultimate proof for *in situ* lacustrine production was the detection of an unusual hexamethylated brGDGT isomer, containing both a 5- and 6-methyl group, in the surface sediments of a Swiss mountain lake but not in surrounding catchment soils (Weber et al., 2015). Moreover, in two Swiss lakes (Weber et al., 2015; 2018) and in two lakes in Greenland (Colcord et al., 2017) the $\delta^{13}C$ values of sedimentary brGDGTs were isotopically distinct from those in surrounding soils, indicating that soils are not a major contributor to the brGDGT pool in these lakes. In light of this, the environmental controls on the distribu-

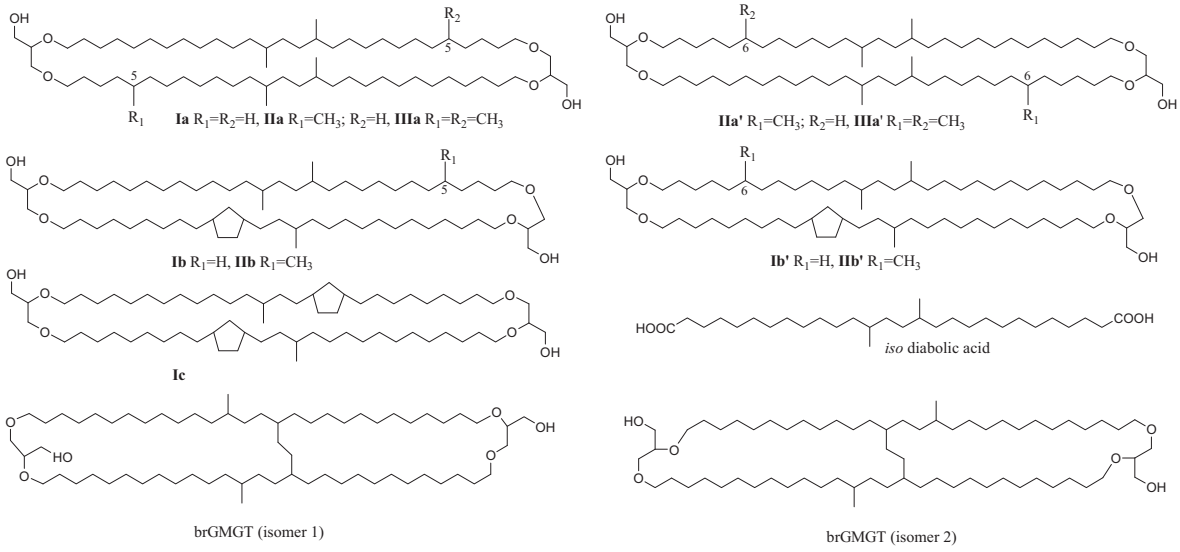

Fig. 1. Molecular structures of brGDGTs and *iso* diabolic acid, and the theoretical structure and configuration of brGMGTs assuming that their structure is similar to that of isoprenoid tetra acids (Lutnaes et al., 2006; 2007) where the bridge is formed by a covalent bond between carbon atoms of two mid-chain methyl groups. The structure of H1020 isomers theoretically resemble brGMGT isomer 1 and 2 as depicted here, whereas H1034 and H1048 have respectively one and two additional methyl groups at yet undetermined positions (but presumably also at C-5 and C-6 like for the brGDGTs).

tion of brGDGTs in lake sediments have been assessed independently to create calibrations specifically applicable to lakes (Tierney et al., 2010; Pearson et al., 2011; Loomis et al. 2011; 2012; 2014; Russell et al., 2018). However, if the brGDGTs in lake sediments come from mixed sources (i.e. soils, the water column, and the sediments) of which the relative contribution logically differs among lakes and may also vary through time, additional uncertainty is introduced to the resulting reconstructions. Moreover, as discussed above, the exact producers of brGDGTs are still largely unknown and could be different in soils and lakes. Until those producers are identified, brGDGT-based paleothermometry remains founded on empirical relations only, without mechanistic understanding of the function of particular membrane features in relation to local environmental conditions. This situation prompts further exploration into other lipid biomarkers that are present in lakes and sensitive to temperature.

The so-called H-shaped GDGTs (H-GDGTs) or glycerol mono-alkyl glycerol tetraethers (GMGTs) are a much less commonly studied group of membrane lipids which have a structure similar to GDGTs, but with an additional connection between the alkyl chains, giving them their 'H-shaped' structure (Fig. 1). Both isoprenoid GMGTs (isoGMGTs) and branched GMGTs (brGMGTs) have been identified. Although the precise structure of GMGTs has yet to be determined, the covalent bond in similarly structured isoprenoid tetra acids is formed between the carbon atoms of two mid-chain methyl groups (Lutnaes et al., 2006; 2007), suggesting that GMGTs may be formed in the same way. This contrasts with an earlier suggestion by Morii et al. (1998) that the bridge of isoGMGTs is formed between a methyl group and the aliphatic chain. It has been theorized that their specific structure is an adaptation to heat stress in order to maintain membrane stability at high temperature, and indeed isoGMGTs were first identified in a hyperthermophilic methanogen (Morii et al., 1998). Subsequently, isoGMGTs with up to six cyclopentane moieties have been identified in both hydrothermal (Schouten et al., 2008a; Knappy et al., 2011; Jaeschke et al., 2012; Jia et al., 2014; Bauersachs and Schwark, 2016; Pan et al., 2016; Sollich et al., 2017; Eickmann et al., 2020) and low-temperature environments (Schouten et al., 2008b; Liu et al., 2012; Naafs et al., 2018; Yang et al., 2019). In support of the theory that lipid bridging is a primary adaptation to heat stress, the abundance of isoGMGTs relative to the total abundance of archaeal lipids was found to increase along a temperature gradient in marine hydrothermal sediments (Sollich et al., 2017), and temperature (along with pH) appeared to be an important factor controlling the abundance and variation of isoGMGTs in a hot spring in Tengchong, China (Jia et al., 2014). Additionally, in a set of globally distributed peats, the abundance of isoGMGTs relative to the isoGDGTs (%isoGMGT) was found to generally be higher in peats from areas with higher MAAT (Naafs et al., 2018).

In contrast to the isoGMGTs, brGMGTs have not been identified in prokaryotic cultures and variations with cyclopentane moieties have not yet been discovered. BrGMGTs with $[M + H]^+$ ions m/z 1020 (therefore named H1020) were first detected in marine sediments (Liu et al., 2012; Xie et al., 2014). More recently, a larger diversity of brGMGTs have been identified in peats (Naafs et al., 2018) and lake sediments (Baxter et al., 2019), which likely represent ether-bound alkyl chains with two (H1020; Fig. 1), three (H1034) or four (H1048) methyl groups, if

the bridge is indeed formed through the bonding of two mid-chain methyl groups. Nonetheless, these structures, including the position of the presumed methyl groups, have not yet been confirmed by rigorous chemical characterization. As was observed for the isoGMGTs, the abundance of brGMGTs relative to the brGDGTs (%brGMGT) was found to generally be higher in peats from areas with higher MAAT (Naafs et al., 2018). Moreover, as is the case in brGDGTs, the degree of methylation of brGMGTs in peats is strongly correlated to MAAT (Naafs et al., 2018). To date only few studies have investigated changes in brGMGT abundance or distribution through geological time. Namely, in deep-sea sediments from the Arctic Ocean %brGMGT increased across the Paleocene-Eocene Thermal Maximum, a known period of strong global warming (Sluijs et al., 2020); and in two late Quaternary peat sequences from northeast China higher %brGMGT values were generally also associated with higher MAAT (Tang et al., 2021), with values for the latter based on the brGDGT-temperature calibration of Naafs et al. (2017b). In a set of surficial sediments from an altitudinal transect of 70 tropical lakes in East Africa, %brGMGT was also found to be higher on average in the low-elevation lakes (i.e., those experiencing higher MAAT; Baxter et al., 2019). Notably, brGMGTs in the studied African lake sediments and in the Arctic Ocean sediments have a greater structural diversity than those in peats, which hypothetically could relate either to a different configuration of the bridge or to an alternative position of methyl groups (Fig. 1; Baxter et al., 2019). Although the exact position of the bridge and methyl groups is still unknown, the distribution of the various brGMGTs in the set of East African lake sediments was significantly influenced by local temperature (Baxter et al., 2019).

In order to better understand where in lakes the brGMGTs are produced, how they are integrated into lake sediments and by which aspects of climate they are influenced, we here analyze the occurrence and distribution of brGMGTs in the soils, water column, and surficial lake-bottom sediments of Lake Chala, a permanently stratified crater lake in tropical Africa. Suspended particulate matter (SPM) was collected for 17 consecutive months at 8 different depths between the lake surface and 80 m, and settling particles were collected for 53 consecutive months at a depth of 35 m. Data from a long-standing monitoring program documenting the lake's water-column conditions over the period of sample collection is available for comparison (Sinninghe Damsté et al., 2009; Buckles et al., 2014; van Bree et al., 2018), making this an ideal dataset to identify the source(s) of brGMGTs in lake sediments, to test the potential impact of seasonality and lake mixing on lipid production, and to assess the applicability of the recently developed brGMGT-based MAAT calibrations.

2. MATERIALS AND METHODS

2.1. Study system

Lake Chala (locally "Challa", after a nearby village) is a permanently stratified (meromictic) crater lake located at the base of Mt. Kilimanjaro on the border of Kenya and Tanzania (3°19′ S, 37°42′ E, ~880 m above sea level). It is relatively small (4.2 km^2) and 90–92 m deep with modest seasonal and inter-annual variation. Mean monthly air temperature (MMAT) is generally highest during January-February (25–27 °C) and lowest during July-August (20–21 °C). Annual rainfall at Lake Chala (600 mm yr^{-1}) is exceeded by lake surface evaporation (1700 mm yr^{-1}). The lake's hydrological budget is maintained mostly by groundwater inflow, which originates as rainfall on the montane forest and subalpine zones of Mt. Kilimanjaro (Payne, 1970; Hemp, 2006; Bodé et al., 2020), and to a lesser extent by rainfall on the lake surface and the steep-sided surrounding crater basin. In addition, exceptionally rainy episodes activate a small creek breaching the northwest corner of the crater rim (Buckles et al., 2014; Meyer et al., 2020). Seasonal precipitation patterns at Lake Chala are determined by the bi-annual passing of the Intertropical Convergence Zone (ITCZ) and associated rain belt across the area, which creates an alternation of wet and dry conditions. Lake Chala, therefore, experiences two rainy seasons per year, from March to mid-May (long rains) and from late October to December (short rains). Following the long rains, the main dry season occurs from June to September and is typified by lower air temperature and higher wind speeds, which promotes deep mixing of the water column and injects oxygenated waters down to a depth of ~40–60 m. A second dry and windy interval from late December to February coincides with the annually highest air temperature, and hence leads to more modest mixing (to ~20–25 m depth). Mixing periods introduce nutrient-rich water to the epilimnion and consequently June to October is the period of highest lake productivity (Wolff et al., 2011; Buckles et al., 2014; van Bree et al., 2018). Monitoring of water-column properties such as temperature, pH, conductivity, and dissolved oxygen was carried out in 2013–2014 and is described by van Bree et al. (2018). In addition, the temperature of the water column was measured by automatic loggers between September 2010 and January 2015 (van Bree et al., 2020).

2.2. Sample collection

2.2.1. Suspended particulate matter

The method for collection of SPM profiles has been described in detail by van Bree et al. (2018). In brief, 5 or 10 L of water were collected at 13 depths throughout the water column on a monthly basis between September 2013 and January 2015. These samples were filtered on pre-combusted glass fiber GF/F filters (142 mm diameter, Whatman), stored frozen and subsequently freeze-dried prior to analysis. SPM sampling was carried out at the start of each month, and is here shown as representing the entire month; for example, sampling on 07-09-2013 represents September 2013, and sampling on 30-09-2013 represents October 2013 (see Table S1). For this study we selected SPM from 8 different depths (0, 10, 25, 35, 50, 60, 70 and 80 m) for each sampled month, and additionally at 20, 30, 40 and 45 m for November 2013 and August 2014 (total $n = 141$).

2.2.2. Sediment trap

Collection of sediment-trap samples in Lake Chala has been described previously by several studies (Sinninghe Damsté et al., 2009; Buckles et al., 2014, 2016; van Bree et al., 2020). To summarize, a UWITEC double-funneled sediment trap of 86 mm diameter was first installed in November 2006 at a depth of 35 m in the middle of Lake Chala to collect settling particles. Over the next eight years the sediment trap was emptied at approximately monthly intervals. After collection, the material was allowed to settle for two days before being emptied of excess water and stored frozen. The samples were then thawed and filtered over pre-weighed and pre-combusted (400 °C, 5 h) glass fiber GF/F filters (110 mm diameter, Whatman), stored frozen and freeze-dried prior to analysis. This study focuses on the brGMGTs collected from the period September 2010 until January 2015 (n = 53; Table S2).

2.2.3. Soils

Soil samples used in this study (n = 7) were collected by Buckles et al. (2014) from various locations within and around the crater catchment of Lake Chala, namely deep and organic volcanic soils inside the lakeshore forest; shallow and low-organic volcanic soils higher up on the inner crater slope and on top of the crater rim; deep but low-organic red lateritic soils in the savanna hinterland outside of the crater, and similarly low-organic red soil material which was flushed from the hinterland into the ravine which breaches the crater rim in its northwestern corner (Table S3). These four distinct soil types were identified through cluster analysis of a total of 32 soil samples based on their organic-carbon content (%OC) and the concentration and distribution of brGDGTs (Buckles et al., 2014).

2.2.4. Surficial lake-bottom sediments

Surficial lake-bottom sediments were collected by Buckles et al. (2014) in January-February 2010, by gravity coring at three different water depths along a transect from opposite the creek inlet towards the depocenter of the lake (CH10-10G: 64.7 m; CH10-09G: 75 m and CH10-06G: 91.6 m; see Table S4). All three core sites are in anoxic bottom areas situated well below the oxycline throughout the year. This study used sediment samples from just below the intact sediment–water interface (2–5 cm core depth). Lipid biomarker concentrations were normalized to organic-carbon mass (g OC) using available data on the organic-carbon content of the local 'core-top' interval (0–1 cm) corrected for the down-core trend in organic-carbon content in a similar deep-water gravity core analyzed by Buckles et al. (2016). These bottom-sediment samples each represent an integrated signal from ~30 years of late 20th-century deposition (Verschuren et al., 2009; Blaauw et al., 2011). Sample storage and preparation is described in detail by Buckles et al. (2014).

2.3. Sample preparation and lipid extraction

An in-depth description of lipid extraction from SPM, sediment-trap particles, surficial bottom sediments, and soils is given by Buckles et al. (2014) and van Bree et al. (2018, 2020). In short, the freeze-dried SPM filters were cut in small pieces and extracted by modified Bligh-Dyer method (Bligh and Dyer, 1959). The extracts were then acid-hydrolyzed using 1.5 N hydrochloric acid (HCl) in methanol (MeOH). The samples were refluxed at 80 °C for 2 hours, the pH was modified to 4–5 with KOH / MeOH, and washed three times with DCM. The combined supernatant was dried over a Na_2SO_4 column and dried under N_2 gas. This total lipid extract (TLE) was then separated on an activated Al_2O_3 column into apolar, neutral and polar fractions, using hexane:dichloromethane (Hex:DCM; 9:1, v/v), DCM, and DCM:methanol (DCM:MeOH; 2:1, v/v) as eluents, respectively. For the sediment-trap material, the freeze-dried filters were cut in small pieces and directly extracted by acid hydrolysis to obtain TLEs which were then processed by the same methods as the SPM TLE described above. The lake sediments and soils were extracted and processed in the same way as the SPM.

A known amount of internal standard (99 ng C_{46} GDGT; Huguet et al., 2006) was added to the polar fraction of the SPM, settling particles, lake sediments and soils for quantification. In preparation for liquid chromatography, all polar fractions of SPM, sediment trap, surficial bottom sediments and soils were re-dissolved in hexane:isopropanol (99:1, v/v) and passed over a 0.45 μm polytetrafluoroethylene (PTFE) filter.

2.4. Instrumental analysis

Instrumental analysis of the polar fraction of the SPM, sediment trap, soils and surficial bottom sediments was performed with an Agilent 1260 Infinity ultrahigh performance liquid chromatography (UHPLC) system coupled to an Agilent 6130 single quadrupole mass detector following the method of Hopmans et al. (2016) and described in detail by van Bree et al. (2020). The brGMGTs were detected by their $[M + H]^+$ ions at *m/z* 1020, 1034 and 1048 and elute around 20 min later than the brGDGTs with the same molecular mass. Identification of the different brGMGTs was achieved by comparison of peak retention time with that of known brGMGTs (Baxter et al., 2019). Peak area integration of brGMGTs was carried out using Chemstation (soil, sediment) or Agilent Masshunter (SPM, settling particles). A peak area of $1 * 10^3$ units was determined as the minimum for peaks to be clearly defined with ample separation from the baseline; peaks with smaller areas were excluded. For calculation of brGMGT abundance, peak areas were compared to the internal standard (*m/z* 744), assuming a comparable response of the mass spectrometer for all brGMGTs.

2.5. Proxy calculation

BrGMGTs with $[M + H]^+$ ions *m/z* 1020, 1034 and 1048 are labeled as H1020, H1034 and H1048 respectively, with presumed isomers indicated by a suffix letter (a-c) following the order in which they elute (Baxter et al., 2019). The relationship between the distribution of these isomers in surficial bottom sediments of East African lakes and local MAAT is

captured in the brGMGT Index (brGMGTI): a ratio between the relative abundance of brGMGT isomers which are strongly positively (H1020c, H1034a and H1034c) and negatively (H1020b and H1048) related to MAAT.

$$\text{brGMGTI} = \frac{[\text{H1020c}] + [\text{H1034a}] + [\text{H1034c}]}{[\text{H1020b}] + [\text{H1020c}] + [\text{H1034a}] + [\text{H1034c}] + [\text{H1048}]} \quad (1)$$

MAAT was estimated using the two temperature models of Baxter et al. (2019), based either on correlation between the brGMGTI and temperature (Eq. (2): $r^2 = 0.94$):

$$\text{MAAT} = 2.86 + 26.5 * \text{brGMGTI} \quad (2)$$

or on stepwise forward selection (SFS), a statistical technique which sequentially selects the brGMGTs whose relative abundance most significantly correlates with MAAT in the East African lake data set (Eq. (3): $r^2 = 0.94$; see also Loomis et al., 2012; Russell et al., 2018):

$$\text{MAAT} = 1.18 + 0.47 * [\text{H1034a}] + 0.12 * [\text{H1020a}] + 0.50 * [\text{H1020c}] \quad (3)$$

The summed abundance of all brGMGTs relative to that of all brGDGTs is calculated following Naafs et al. (2018):

$$\%\text{brGMGT} = \frac{\Sigma\text{brGMGT}}{\Sigma\text{brGMGT} + \Sigma\text{brGDGT}} * 100 \quad (4)$$

2.6. Statistical analysis

To evaluate brGMGT variability in the different settings, principal component analysis (PCA) of the fractional abundances was performed using the R statistical package FactoMineR (Lê et al., 2008). For SPM, the mean fractional abundance of the individual brGMGTs was weighted to the summed brGMGT (∑brGMGT) concentration for each sample (in ng L^{-1}). Likewise, for soils and surficial bottom sediments the mean fractional abundances were weighted to ∑brGMGT concentration (μg g^{-1} OC). For settling particles, the mean fractional abundance of the brGMGTs was weighted to ∑brGMGT flux for each sample (in ng m^{-2} day^{-1}).

3. RESULTS

3.1. Spatial and temporal distribution of brGMGTs in SPM

BrGMGTs were above the detection limit in the majority of SPM samples collected monthly between September 2013 and January 2015 (109 out of 141 samples; 77.3%). The maximum ∑brGMGT concentration of 0.61 ng L^{-1} was reached in April 2014 at a depth of 60 m (Fig. 2h),

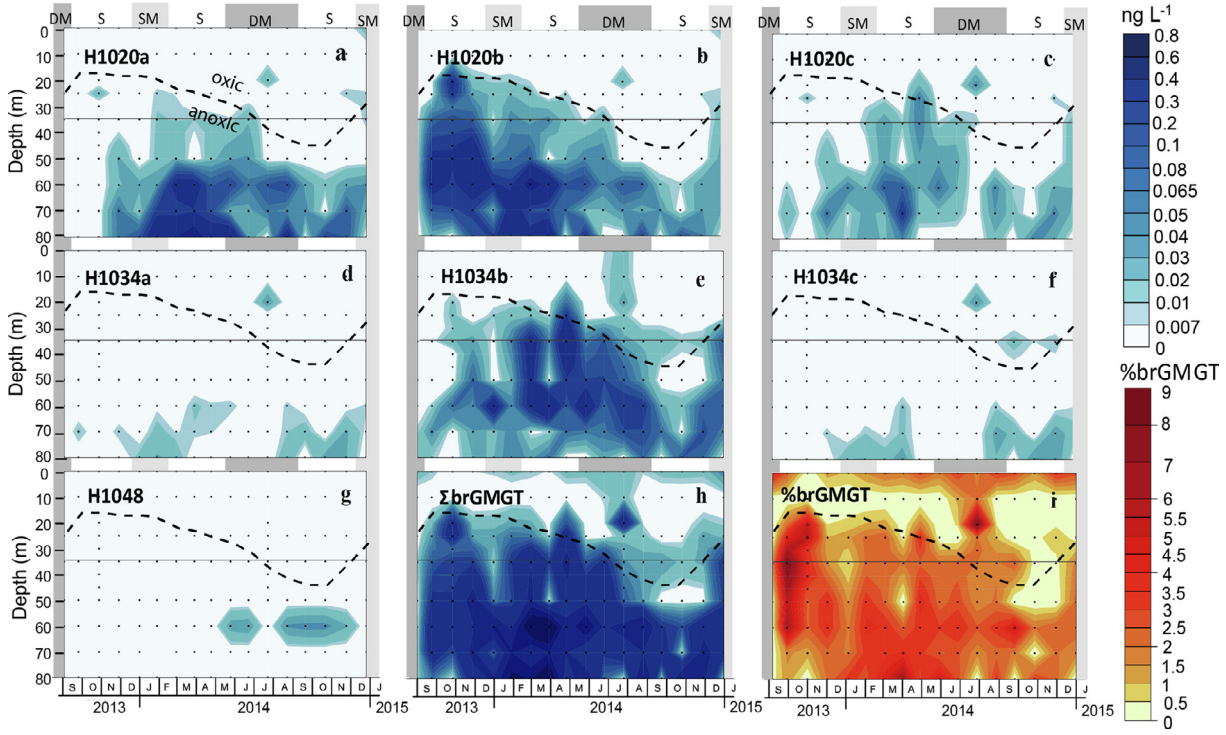

Fig. 2. Interpolated concentrations (in ng L^{-1}) of the seven known brGMGTs (a-g) and their summed total (h) in SPM from the water column of Lake Chala, sampled at approximately monthly intervals between September 2013 and January 2015. The %brGMGT values (i) are calculated using Eq. (4) (see Methods). Grey background shading indicates the intervals of shallow (SM) and deep mixing (DM) of the water column. The overlying dashed black line indicates the depth of the oxycline, and the fine grey horizontal line the depth of the sediment trap collecting settling particles.

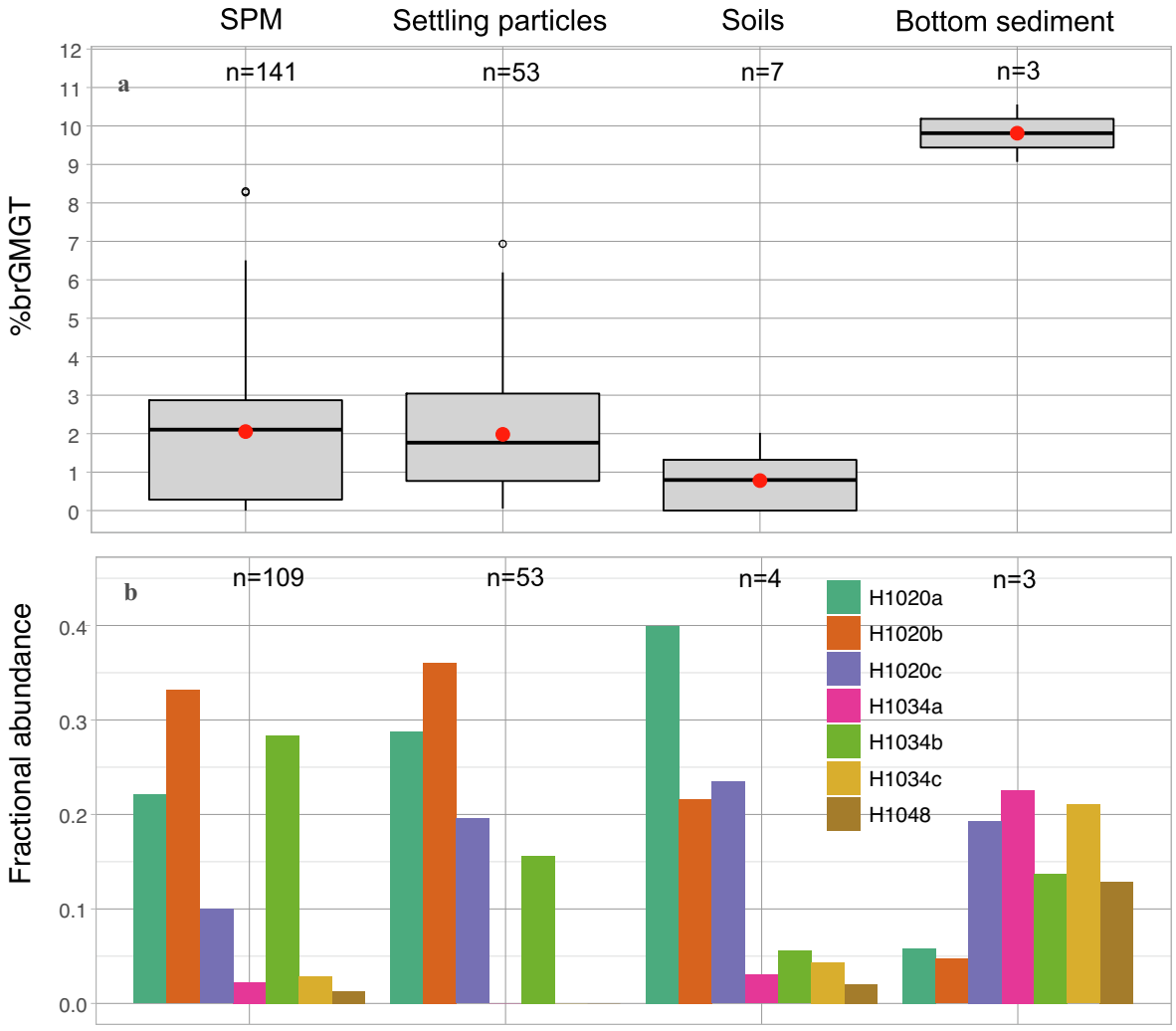

Fig. 3. (a) Boxplot of %brGMGT values across all available samples from each of the four sample types in and around Lake Chala: suspended particulate matter (SPM), settling particles, soils and surficial lake-bottom sediments. Indicated are the median (bold black line) and average (red dot) values, and the first and third quantiles (lower and upper hinges), with whiskers (thin lines) extending up to 1.5× the interquartile range (IQR) from the hinge to the maximum/minimum value, and outliers (open black circles) defined as data points beyond 1.5 × IQR. (b) Mean fractional abundances of each of the seven known brGMGTs in the four system components. The mean fractional abundances are weighted to ΣbrGMGT flux (ng m^{-2} day^{-1}) for the settling particles, and to the ΣbrGMGT concentration for the SPM (ng L^{-1}), soils (μg g^{-1} OC) and surficial bottom sediments (μg g^{-1} OC).

six times higher than the overall average (0.10 ng L^{-1}). ∑brGMGT was generally two orders of magnitude lower than ∑brGDGT, which averaged 4.0 ng L^{-1} and reached a maximum of ~24 ng L^{-1} (van Bree et al., 2020). This results in %brGMGT values ranging from 0 to 8.3%, with an average of 2.1% throughout the SPM record (Fig. 2i; 3a). The ΣbrGMGT concentration in SPM normalized to each sample's particulate carbon (PC) content averages 1.4 μg g^{-1}C (n = 141). The PC values used here include both inorganic and organic carbon, but mostly represent living or dead phytoplankton and heterotrophic aquatic microbiota (van Bree et al., 2018) and can therefore reasonably substitute for OC.

Throughout the 17-month SPM interval, brGMGTs were generally most abundant in the anoxic zone of the water column and often below detection limit in the oxygenated upper layer. During the periods immediately following shallow mixing (January 2015) and deep mixing (June-September 2014; van Bree et al., 2018), brGMGTs were largely concentrated below depths of ~35 m and ~50 m, respectively (Fig. 2h). Conversely, during periods of stronger stratification (e.g. October-November 2013 and April-May 2014), relatively higher brGMGT concentrations extended up to a depth of ~20 m. In accordance, depth-integrated concentrations over the entire water column were highest when the water column was strongly stratified, and lowest at the end of the deep mixing period in 2014 when the oxycline reached its maximum depth at ~45 m (Fig. 4a).

All seven brGMGTs previously detected in East African lake sediments (Baxter et al., 2019) were identified in the SPM of Lake Chala (Fig. 2a-g). However, brGMGTs

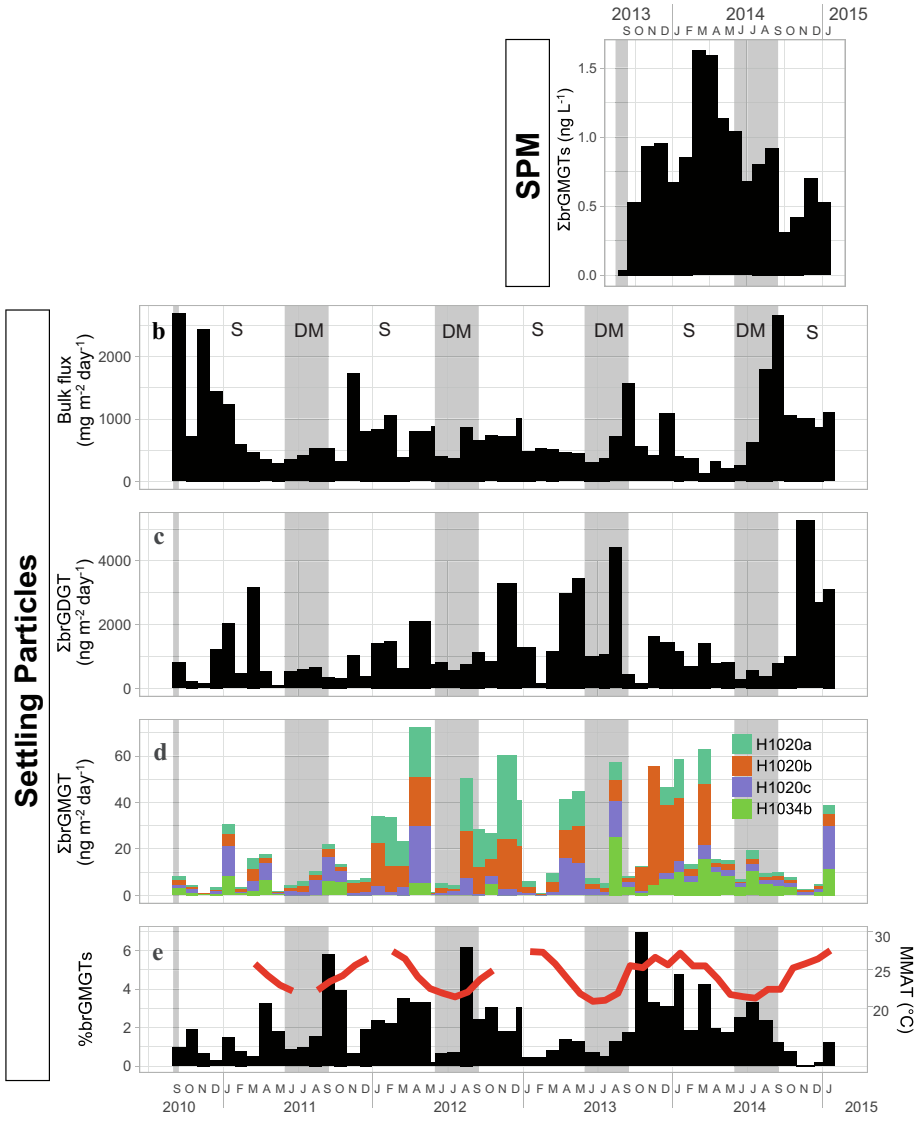

Fig. 4. (a) Depth-integrated concentration of ΣbrGMGT (ng L^{-1}) in SPM from Lake Chala, sampled monthly from September 2013 to January 2015. (b-e) Time series of particles settling in the sediment trap suspended at 35 m depth, collected monthly from September 2010 to January 2015: (b) total bulk dry flux (mg m^{-2} day^{-1}); (c) total brGDGT flux (ΣbrGDGT, in ng m^{-2} day^{-1}); (d) total brGMGT flux (ΣbrGMGT, in ng m^{-2} day^{-1}) with the different colors indicating the proportions of the individual brGMGTs; and (e) %brGMGTs calculated using Eq. (4) (see Methods). The thick red line represents monthly mean air temperature (MMAT) measured at a nearby (~25 km) savannah site (data from Bodé et al., 2020). Background shading highlights the seasonal alternation of water-column stratification (S; here including shallow mixing) and deep mixing (DM).

H1034a, H1034c and H1048 were often below detection limit and their presence was limited almost exclusively to depths ≥ 60 m. They appear in 20%, 21% and 4% of the SPM samples, respectively. Of the remaining brGMGTs, H1034b was most commonly detected (68%), followed by H1020b (64%), H1020a (54%) and H1020c (53%). H1020a had the highest maximum concentration during the studied interval, reaching 0.28 ng L^{-1}, followed by H1020b (0.26 ng L^{-1}), H1034b (0.22 ng L^{-1}), H1020c (0.10 ng L^{-1}), H1048 (0.035 ng L^{-1}), H1020c (0.033 ng L^{-1}) and H1034a (0.030 ng L^{-1}; Fig. 2a-g).

Although all brGMGTs increase in concentration below the oxycline, the distribution of the individual brGMGTs in the water column show marked spatial and temporal differences (Fig. 2a-g). For example, H1020b is the most abundant brGMGT during stratified conditions in September-December 2013, whereas H1034b and H1020c dominate the water column during similarly stratified conditions in March-May 2014. Although the temporal patterns of H1034b, H1020c and H1020a are similar, H1020a shows greater concentrations at depths of ≥ 60 m, while H1034b and H1020c appear in relatively high concentrations in the 40–60 m depth range. H1048, H1034a and H1034c occur almost exclusively in the deepest water (≥60 m). The distribution of H1034a and H1034c is mostly scattered, while H1048 appears only during the mixing period when the oxycline is deepening.

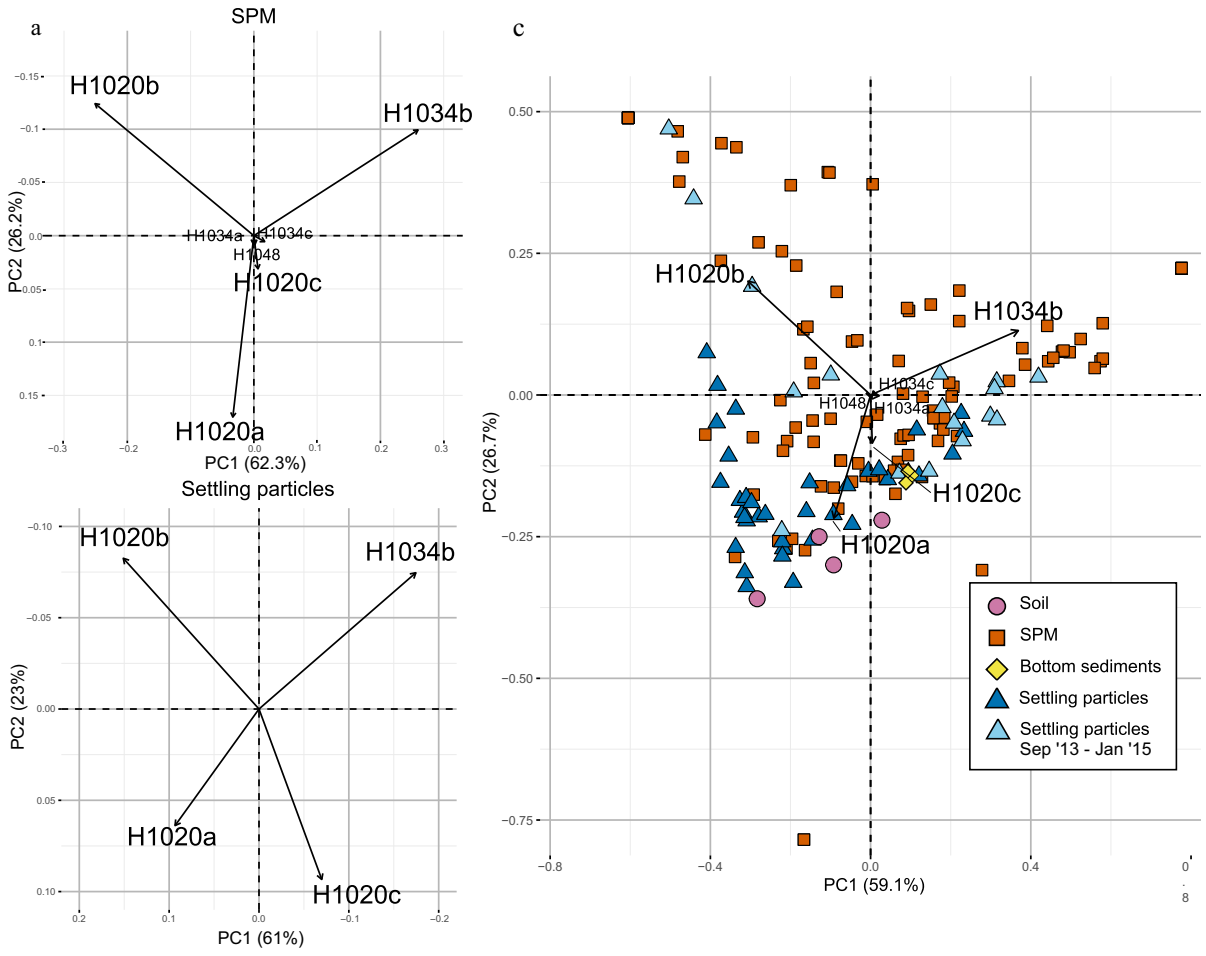

Fig. 5. Principle component analyses (PCAs) of the fractional abundances of the seven known brGMGTs in the sampled SPM (a; n = 109) and settling particles (b; n = 53) from Lake Chala, and of the combined data set (c; n = 162) with the position of individual samples along PC1 and PC2. In (a) and (b), either PC2 or both axes were reversed to conserve the general orientation of the black vectors indicating the PCA scores of individual brGMGTs. In (c), light blue triangles indicate settling-particle samples from the 17-month period overlapping with the SPM data set, and PCA scores for soils (pink circles) and surficial bottom sediments (yellow diamonds) were added passively.

Overall mean concentration-weighted fractional abundances were calculated on the basis of all SPM samples containing at least one brGMGT compound above detection limit (n = 109). H1020b had the highest fractional abundance overall (0.33), followed by H1034b (0.28), H1020a (0.22), H1020c (0.10), H1034c (0.029), H1034a (0.023) and H1048 (0.013; Fig. 3b). Hence, the brGMGT assemblage is dominated by four compounds, namely the three H1020 isomers and H1034b. Because of the marked differences in spatial and temporal distribution (Fig. 2a-g), also the fractional abundances of individual brGMGTs in the SPM varied substantially with depth and through time (Table S1). Temporal and depth-related variation in the fractional abundance of individual brGMGTs among SPM samples was further investigated using PCA (n = 109; Fig. 5a). Together, PC1 and PC2 explain 89% of the total observed variation, which is mainly driven by the fractional abundances of the three most abundant brGMGTs: H1020b, H1034b and H1020a. On PC1, which explains 62% of the variation, H1034b loads strongly positively, while H1020b loads strongly negatively. PC2 explains 26% of the variation, with H1020b and H1034b having a strong negative loading and H1020a a strong positive loading. Compared with these three brGMGTs, the positive loading of H1020c on PC1 and PC2 is decidedly modest.

3.2. Temporal variation in brGMGTs from settling particles

BrGMGTs were detected in all samples of settling particles, trapped at a depth of 35 m on a monthly basis from September 2011 to January 2015 (n = 53; Table S2). ∑brGMGT flux varied by two orders of magnitude, i.e. from 0.71 ng m^{-2} day^{-1} (in February 2013) to 72 ng m^{-2} day^{-1} (in April 2012; Fig. 4d). Notably, the ∑brGMGT flux shows no correlation with the bulk particle flux ($r^2 = 0.009$) or with the ∑brGDGT flux ($r^2 = 0.095$; Fig. 4-b-d). The %brGMGT in settling particles was ~2% on average (Fig. 3a), ranging from 0.05% (November 2014) to almost 7% (October 2013), and does not show a clear trend with mean monthly air temperature (MMAT; Fig. 4e).

Only four of the seven brGMGTs previously identified in East African lake sediments (Baxter et al., 2019), and in Lake Chala SPM (Section 3.1), were detected in the settling-particle samples. These are, in order of frequency, H1020b, H1020a, H1020c (which were almost always detected) and H1034b (present in 57% of the samples), with maximum fluxes of 52, 36, 25 and 25 ng m^{-2} day^{-1}, respectively. Across the entire time series, H1020b had the highest mean flux-weighted fractional abundance (0.36), followed by H1020a (0.29), H1020c (0.20) and H1034b (0.16; Fig. 3b). However, both the fluxes and fractional abundances of each brGMGT varied significantly over time. In the first 16 months of the monitored interval, from September 2010 to December 2011, the ∑brGMGT flux was relatively low (on average 9.8 ng m^{-2} day^{-1}) and was not dominated by any individual brGMGT. During the next 19 months, from January 2012 to July 2013, the ∑brGMGT flux was generally higher (on average 26 ng m^{-2} day^{-1}) and H1034b was most often absent (on average 2.1 ng m^{-2} day^{-1} and a fractional abundance of 0.17), while H1020a and H1020b were more fractionally abundant (on average 0.22 and 0.26, respectively). For the remaining 18 months, from August 2013 until January 2015, the ∑brGMGT flux remained high (on average 25 ng m^{-2} day^{-1}) but H1034 reappeared with an average fractional abundance of 0.34, while H1020a was greatly reduced (on average 3.9 ng m^{-2} day^{-1} and a fractional abundance of 0.16). Also from October 2013 to January 2014, H1020b experienced a significant peak in flux (on average 30 ng m^{-2} day^{-1}) and fractional abundance (on average 0.71).

The PCA on the fractional abundance of the four brGMGTs recovered from settling particles (n = 53) is shown in Fig. 5b. PC1 and PC2 together explain 84% of the observed variation in this dataset, comparable to the value for SPM (89%). PC1 captures 61% of the variation, with strong positive loadings of H1034b and H1020c and strong negative loadings of H1020a and H1020b. PC2 captures 23% of the variation and separates H1020a and H1020c, which load strongly positively, from H1034b and H1020b, which load strongly negatively. The results of a PCA on the combined data sets of SPM and settling particles (n = 162; Fig. 5c) are highly comparable to those of the individual data sets (Fig. 5a-b).

3.3. Distribution of brGMGTs in catchment soils

BrGMGTs were detected in only four of the seven soil samples analyzed (Fig. 6; Table S3). These samples either represent deep but low-organic red savanna soils (J9, J11) and similar red soil material collected from the creek bed near the lakeshore (LB80), or low-organic grey soil from halfway up the inner crater slope (J1; Buckles et al., 2014). The three samples in which brGMGTs were not detected have diverse origins: one is from highly organic forest soil on the eastern lakeshore (J3), one from shallow grey volcanic soil on top of the crater rim (LB74), and one from red savanna soil some km to the west of Chala crater (LB85). Only one of the analyzed soil samples (J9) contained all seven known brGMGTs. The other three soil samples with brGMGTs (J1, J11 and LB80) contained only the three isomers of H1020 (Fig. 6). The total brGMGT concentration in the analyzed soils ranged from 0 to 0.28 μg g^{-1} OC, with an overall average of 0.08 μg g^{-1} OC, and the maximum %brGMGT was 2.0% (n = 7; Fig. 3a). In the four soils containing brGMGTs, when

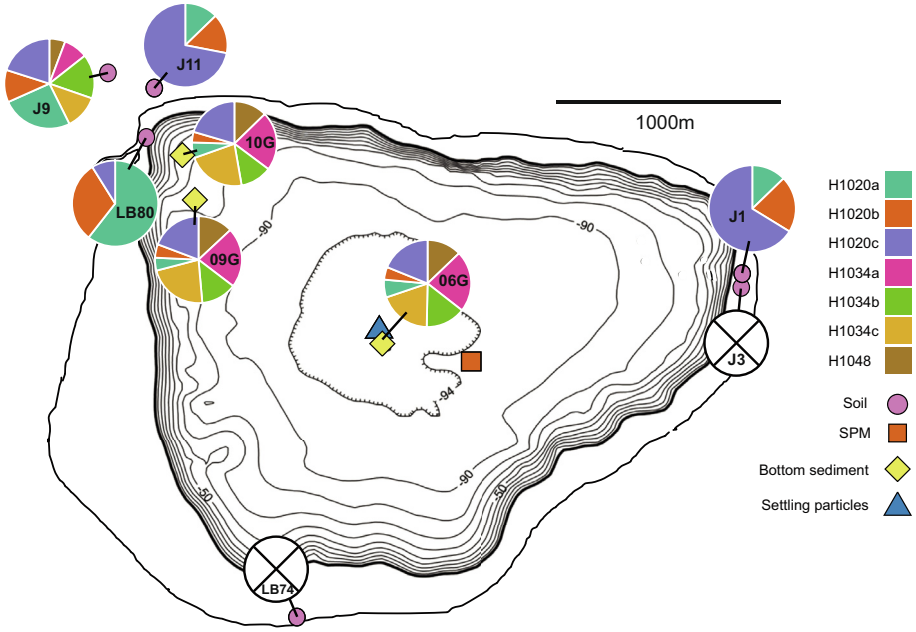

Fig. 6. Map of the Chala crater basin (outer thick black line) and bathymetry of Lake Chala (depth contours; from Moernaut et al., 2010) with sampling locations of the SPM, settling particles, soils and surficial bottom sediments analyzed in this study. Fractional abundances of the brGMGTs recovered from individual soil and bottom-sediment samples are shown in accompanying pie charts; in soils marked with a black X, no brGMGTs were detected. One soil sample (LB85) lacking brGMGTs lies outside the map limits and is not shown.

weighted to ∑brGMGT concentration, H1020a had on average the highest fractional abundance (0.40), followed by H1020c (0.23) and H1020b (0.22; Fig. 3b). The average fractional abundances of H1048 and H1034a-c were all < 0.06 because they were either rare or lacking in individual samples.

3.4. Distribution of brGMGTs in surficial lake-bottom sediments

All seven brGMGTs were detected in the three analyzed samples of surficial sediment from the profundal lake bottom (Table S4). The ΣbrGMGT concentration was on average 1.05 μg g^{-1} OC (n = 3) and increased about three-fold from the lake's periphery (0.54 μg g^{-1} OC) to its depocenter (1.41 μg g^{-1} OC). The %brGMGT of these three bottom sediments did not vary substantially (9.1–12.5%) and was on average 10.7% (Table S4), by far the highest average %brGMGT value recorded among the four studied sample types (Fig. 3a). The fractional abundance of individual brGMGTs in the bottom sediments was also highly consistent among the three locations (Fig. 6). H1034a generally had the highest fractional abundance (0.23), followed closely by H1034c (0.21) and H1020c (0.19), thereafter by H1034b (0.14) and H1048 (0.13), and finally H1020a (0.06) and H1020b (0.05; Fig. 3b). Notably, the fractional abundance of H1034a, H1034c and H1048 is higher in the surficial bottom sediments than in either the SPM, settling particles or soils, where they are (mostly) below detection limit.

4. DISCUSSION

4.1. Sources of brGMGTs in the water column

Comparison of the brGMGT distributions in SPM and settling particles can determine if the brGMGTs in the water column (as represented by SPM) are produced in the lake or are derived from terrestrial soil material flushed into the lake through rain-induced erosion and overland flow. Whereas SPM data may be described as a snapshot of particle distribution at the moment of collection, settling particles captured by the sediment trap have accumulated over the course of an entire month, and can therefore be expected to also include washed-in terrestrial material. Yet, the average distribution of brGMGTs in SPM and settling particles is quite comparable, both being dominated by the same four brGMGTs (H1020a-c and H1034b; Fig. 3b). Likewise, the PCA results for SPM and settling particles are highly similar (Fig. 5). By contrast, the analyzed soils had a markedly different brGMGT composition than the former two sample types. Namely, the %brGMGT of the soils is significantly lower ($p < 0.01$), and while H1034b is relatively scarce the fractional abundance of H1020a is much higher. Lack of (detectable levels of) brGMGTs in three of the seven soils certainly indicates that they are not ubiquitous in soil. The average ∑brGMGT concentration in soils (0.08 μg g^{-1} OC) is 17.5 times lower than in the SPM (1.4 μg g^{-1} PC), strongly suggesting that brGMGTs in the latter are produced within the lake system. Altogether, this indicates that brGMGTs in the SPM and settling particles have a shared aquatic source (and/or shared environmental drivers), with minimal contribution of soil-derived brGMGTs washed into the lake. This is comparable to what was previously reported for the brGDGTs in Lake Chala (Buckles et al., 2014; van Bree et al., 2020) and is in line with the general absence of terrestrial biomarkers, such as long-chain *n*-alkanes, in the SPM during the studied interval (van Bree et al., 2018). Likewise, brGMGTs in geothermally heated soils (De Jonge et al., 2019) and soils from an elevation transect in the Peruvian Andes (Kirkels et al., 2020) were most often below detection limit, while brGDGTs were found in high abundance.

The spatiotemporal distribution of brGMGTs in the SPM (Fig. 2) further elucidates their aquatic origin. Based on a single SPM profile through the water column of Lake Chala it had previously been suggested that the elevated concentrations of GDGTs in the lower water column related to the better preservation of organic matter in anoxic conditions (Sinninghe Damsté et al., 2009; Buckles et al., 2014). By this reasoning, brGDGTs and other stable biomolecules might accumulate over time after sinking below the oxycline, where they are more neutrally buoyant and less likely to be removed from the water column by aggregation or grazing (Sinninghe Damsté et al., 2009; Buckles et al., 2014). However, strong spatial and temporal variation in the concentration and distributions of brGMGTs in Lake Chala SPM, even within the anoxic zone (Fig. 2), rather implies the existence of distinct ecological niches of different brGMGT producers. Although there is some indication that brGMGTs were redistributed into the oxygenated upper water column as a result of deep mixing in July-August 2014 (Fig. 2; 4a), also during this interval they are still predominantly concentrated below the oxycline, indicating that brGMGT producers presumably favor anoxic conditions. This implies that the spatial and temporal pattern of brGMGTs in the SPM is more strongly determined by the distinct niches occupied by particular species or communities of bacteria producing brGMGTs, while they are controlled only indirectly by the physical process of lake mixing and stratification. Similarly, van Bree et al. (2020) also proposed *in situ* production of brGDGTs in Lake Chala based on their spatial and temporal variation in the SPM.

4.2. Seasonal variation in brGMGTs in the water column

During the cool and windy conditions of the main dry season when the oxycline is depressed, the zone of brGMGT concentration in the SPM is more restricted to deeper water (Fig. 2). Conversely, during periods of stronger stratification when anoxia extends to shallower depth, high brGMGT concentrations in the SPM are found higher up in the water column. Thus, brGMGT production is clearly influenced by seasonal changes in water-column stratification and mixing. However, individual brGMGTs behave differently over time and with depth. For example, although H1034b, H1020a, H1020b and H1020c are all more abundant during stratified conditions than during lake mixing, H1020b was the most abundant compound

during the 'short rains' stratified interval of September – December 2013, whereas brGMGTs H1034b, H1020a and H1020b dominated during the 'long rains' stratified interval of March – May 2014. A similar distinction between periods of stratification was also observed for brGDGTs in the same SPM (van Bree et al., 2020). It thus appears that while the presence of dissolved oxygen influences the general abundance of both brGMGTs and brGDGTs in the water column of Lake Chala, other factors determine the relative abundance of these individual lipids.

As total brGMGT abundance in the SPM appears to be linked to the annual cycle of water-column stratification and mixing, we expected that this influence would also be evident in the 53-month-long record of settling particles, which overlaps with the 17-month period of SPM collection (Fig. 4). Indeed, during the concurrent period (September 2014 to January 2015) the two records are in broad agreement, in that the flux of brGMGTs into the sediment trap suspended at 35 m was larger during stratified conditions than during the period of deep mixing (Fig. 4a, c). However, over the entire 53-month time series of settling particles this annual cycle is not apparent, creating doubt on the consistency of brGMGT response to lake mixing and stratification on a multi-annual timescale. Lack of the annual cycle in our settling-particle data may be partly explained by the deployment of the sediment trap at 35 m depth. Selected specifically to optimally capture seasonal water-column dynamics, this depth is either above or shortly below the oxycline (Fig. 2), and as a result the sediment trap has collected brGMGTs from the part of the water column where brGMGT production is low.

Based on previous studies of brGMGTs in peats and East African lake sediments, it can be speculated that besides water-column mixing also temperature should exert some control on brGMGT production in Lake Chala. Specifically, higher %brGMGT values in SPM and settling particles may be expected when ambient air and/or water temperature is higher (Naafs et al., 2018; Baxter et al., 2019). Mean monthly air temperature (MMAT) around Chala crater fluctuates by ~6 °C through the year, and the lake's surface-water temperature by ~5 °C (Buckles et al., 2014; van Bree et al., 2018, 2020), with water temperature slightly lagging trends in air temperature. MMAT peaks in January and is lowest in July (Fig. 4e). The upper mixed layer including the lake surface is warmest during the period of strong stratification in March – May and coolest towards the end of the deep mixing season in August (Buckles et al., 2014; van Bree et al., 2020). However, opposite to expectation the %brGMGT of SPM in the upper water column of Lake Chala is relatively low during the warmest period of the year and is higher during the deep-mixing period (Fig. 2i) when air and mixed-layer temperature are lowest. Most likely this is because peak %brGMGT values result from redistribution of suspended material from lower depths into the surface layer at times of mixing rather than from an influence of temperature on brGMGT production. At the same time, %brGMGT in particles settling from the upper 35 m shows no comparable annual cycle linked to the monitored seasonal variation in temperature or water-column mixing (Fig. 4e). Lacking a feasible explanation for this apparent conflict at present, we propose that it may be related to the difference in sampling techniques, by which SPM represents particle distribution at the discrete moment of collection whereas sediment-trap samples represent the accumulation of material over an entire month. Moreover, assuming that brGMGTs are mainly produced below the oxycline, where temperature remains relatively constant at 22–23 °C throughout the year (van Bree et al. 2018), observed temporal variation in % brGMGT in this part of the water column (Fig. 2i) must be driven by some factor other than temperature. Thus, variation in both absolute brGMGT abundances as well as relative to brGDGTs in the SPM and sediment-trap material cannot be directly linked to temperature at the time scales investigated here.

Besides temperature and dissolved oxygen, other factors including pH (De Jonge et al., 2014; Naafs et al., 2017b; Russell et al., 2018), nutrient availability (Loomis et al., 2014), conductivity (Tierney et al., 2010; Shanahan et al., 2013) and redox boundaries (Weber et al., 2018) have all been discussed as possibly influencing the distribution of the more commonly studied brGDGTs in natural settings. However, in the case of brGMGTs only the influence of pH in peats (Naafs et al. 2018) and lakes (Baxter et al., 2019) has so far been studied empirically, and in neither system was a correlation found. In Lake Chala the oxycline, thermocline and strongest pH gradient most often all occur at similar depths (van Bree et al., 2018), because they are all controlled primarily by the seasonal variation in wind-driven water-column mixing, rendering it difficult to separate their individual effects on brGMGT distribution. Whereas temperature is relatively stable throughout the anoxic zone (Wolff et al., 2014), the increase in dissolved solids with depth responsible for the permanent stratification of Lake Chala (i.e., its meromictic status) is mostly concentrated between ~45 and ~65 m depth (Barker et al., 2013; Wolff et al., 2014), and ~50% of the total pH gradient occurs in the lower half of the water column (Buckles et al., 2014; Wolff et al., 2014). This chemical gradient being a reflection of the increasing water density with depth, the lower water column of Lake Chala can be divided in four zones characterized by their decreasing frequency (or probability) of mixing at multi-annual and longer time scales (Buckles et al. 2014). Moreover, seismic-stratigraphic signatures (Moernaut et al., 2010) and the carbon-isotopic composition of deep-water dissolved inorganic carbon (Barker et al., 2013) both indicate that methane gas produced by post-burial decomposition of organic matter may be released from the lake floor. The combined data suggest the occurrence of a strong redox gradient in the lower water column of Lake Chala controlling the depth-specific distribution of nitrogen compounds and other chemical species (Buckles et al., 2013; Wolff et al., 2014). In turn the chemical and redox gradients may define the depth-specific niches of different brGMGT producers within the ~50 m tall anoxic zone of Lake Chala. For example, we see that brGMGTs H1020a and b occur lower in the water column than 1034b and H1020c, which seem to be produced mainly in the 40–60 m depth range (Fig. 2). Similar patterns were observed in the

brGDGTs, where IIa′ and IIIa′ mainly occurred > 60 m depth, whereas Ib, IIb, and IIa occurred in the 40–60 m zone (van Bree et al., 2020).

4.3. Production of brGMGTs in surficial lake-bottom sediment

The normalized ΣbrGMGT concentration in the SPM of Lake Chala (1.4 μg g^{-1} PC) is higher, on average, than that of surficial lake-bottom sediments (1.05 μg g^{-1} OC). However, the proportion of brGMGTs to brGDGTs in bottom sediments is significantly higher: the %brGMGT in both the SPM and settling particles is on average ~2% (for concentration and flux respectively), whereas in the bottom sediments it is 10.7% (Fig. 3a). Considering as unlikely that preferential preservation of brGMGTs relative to brGDGTs would already have a significant effect in recently deposited anoxic sediments, this high %brGMGT value may reflect *in situ* production of brGMGTs in the sediments. However, as %brGMGT may also depend on the behavior of the brGDGTs it is not a direct indication of sedimentary production. More compelling evidence for sedimentary brGMGT production in Lake Chala is the markedly different distribution of brGMGTs in the bottom sediments compared to that of the SPM and setting particles (Fig. 3b). All seven known brGMGTs occur in the surficial bottom sediments, and particularly H1048, H1034c and H1034a are present in much higher fractional abundance than in the water column. Additionally, as the fractional abundances of individual brGMGTs is highly consistent in recently deposited sediments from three locations spanning a nearshore-to-offshore transect of deep-water lake bottom (Fig. 6), sedimentary brGMGT composition is clearly unaffected by influx of soil-derived brGMGTs via the rim-breaching creek. While it cannot be excluded that the difference in brGMGT distribution between sediment and water-column samples is related to greater temporal integration in the former (~30 years for sediments *versus* 17 months for SPM and 53 months for settling particles), production of brGMGTs in the bottom sediments seems more likely. This suggests that, although brGMGTs represent a slightly greater fraction of organic carbon in the SPM than in the bottom sediments, there is either limited export of these water-column brGMGTs to the sediments *or* the lake floor is highly productive, resulting in a greater proportion of organic material. In conclusion, it appears that sedimentary brGMGTs are mainly derived from production in the permanently anoxic lake-floor sediments, and to a much lesser degree from production in the anoxic lower water column, with possible exclusion of H1020a and H1020b as these two compounds have a higher fractional abundance in the water column than in the sediments (Fig. 3b). This would imply that at least some brGMGTs in lake sediments have a relatively singular source. This contrasts with the situation for brGDGTs in Lake Chala, where comparable distribution in surficial bottom sediments and the water column indicates that sedimentary brGDGTs are most likely derived from mixed sources (van Bree et al., 2020). Significantly, the overall restriction of brGMGTs to the anoxic part of the Chala water column and underlying lake sediments strongly suggests that brGMGT producers cannot cope well with oxygenated conditions and are therefore likely anaerobic bacteria. Following this logic, the majority of brGMGT production in shallow and/or well-oxygenated lakes (e.g., 26 of the 70 lakes in the East African lake calibration are < 5 m deep; Baxter et al., 2019) arguably occurs within their anoxic bottom sediments.

4.4. Implications for the use of brGMGTs as paleoproxies of lake temperature

Before brGMGTs may be confidently used to generate quantitative reconstructions of past temperature, it should be understood how the temperature signal is incorporated and preserved in the lake's bottom sediments. Previously, both %brGMGT and the relative distribution of individual brGMGTs in East African lake sediments were shown to relate to local mean annual air temperature (MAAT; Baxter et al., 2019). The %brGMGT of surficial bottom sediments in Lake Chala (local MAAT = 25 °C) is highly consistent among the three analysed samples (range 9.1 – 12.5%, on average 10.7%; Fig. 3a). This is within the wide range of %brGMGT values (4.2–30.9%) found in other East African lakes at low or modest elevation (<2000 m a.s.l. and local MAAT ranging between ~20 and 28 °C; Fig. 7a). The average brGMGT-inferred estimates of Lake Chala MAAT using the brGMGTI and SFS models of Baxter et al. (2019) are 23.6 and 22.3 °C, respectively, i.e. underestimating the measured value by 1.4 and 2.7 °C (Fig. 7b, c). In both the brGMGTI and SFS models, which have a residual mean square error (RMSE) of respectively 2.16 °C and 2.20 °C, Lake Chala MAAT estimates plot within the cloud of data points derived from low-elevation (hence, warm) East African lakes. Thus, the distribution of sedimentary brGMGTs in Lake Chala, which is not included in the East African lake calibration of Baxter et al. (2019), conforms to expectation. This result confirms the predictive power of the published models, and suggests that they may be reliably applied to subsurface sediments extracted from this lake.

If brGMGTs in lake sediments are mostly produced within the surface sediments themselves, as seems to be the case in Lake Chala, relating brGMGT distribution to local air temperature may introduce some uncertainty to the temperature estimates. In most East African lakes analyzed by Baxter et al. (2019), and near-equatorial lakes in general, bottom-water temperature (BWT) generally does not differ from local MAAT by more than a few degrees (Talling, 1969; Lewis, 1987) because BWT is similar to the annually lowest temperature of the daily mixed layer, and temperature of the mixed layer traces MMAT, which itself varies only a few degrees throughout the year (as little as 1.5 °C in equatorial western Uganda; De Crop and Verschuren, 2019). Therefore, the distribution of sedimentary brGMGTs in these lakes will rather closely reflect local MAAT, at least across the ~25 °C range in local MAAT covered by the East African lakes calibration dataset (Fig. 7). Moreover, the temperature recorded by sedimentary brGMGTs in a shallow unstratifying lake (in tropical

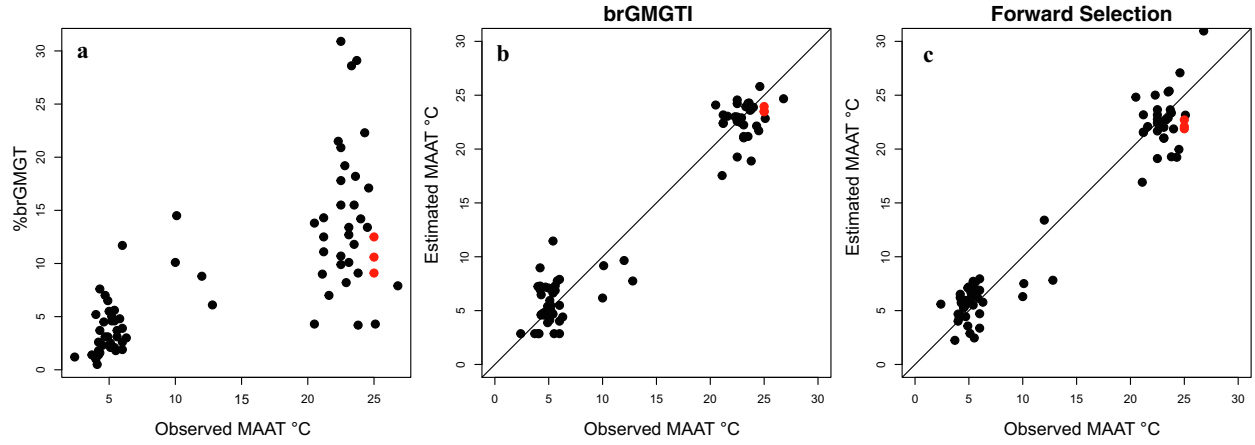

Fig. 7. (a) %brGMGT in surficial lake sediments from an altitudinal gradient of 70 East African lakes *versus* observed local MAAT. (b) MAAT estimated using the brGMGTI *versus* observed MAAT. (c) MAAT estimated using the forward-selection (SFS) method *versus* measured MAAT. All data from Baxter et al. (2019), with values derived from the three Lake Chala bottom-sediment samples added in red (see also Table S4). BrGMGTI, estimated MAAT and %brGMGT were calculated using Eqs. (1)–(4) (see Methods).

regions, shallow lakes are actually polymictic rather than unstratified; Lewis, 1983) and a deep stratifying lake located at the same latitude and elevation will be broadly comparable (i.e., within or close to the 2.2 °C prediction error of the current models), because BWT of the stratifying lake differs at most a few degrees from mean annual water temperature in its mixed layer, while in the polymictic lake the mixed layer extends (almost) to the lake bottom. For example, in present-day Lake Chala BWT is constant at 22.3 °C, whereas the average mixed-layer temperature is 25.3 °C (data from Buckles et al., 2014; van Bree et al., 2018, 2020). Notably, this generalization also applies to meromictic tropical lakes such as Lake Chala, because of heat diffusion from the at least annually mixed lower part of the mixolimnion into permanently stratified bottom waters. This is clearly illustrated by the increase in deep-water temperature of Lake Tanganyika, the world's deepest tropical lake, since the early 20th century in response to anthropogenic global warming (Verburg & Hecky, 2009). Strictly speaking, in East African (and other near-equatorial) lakes brGMGTI should be more strongly correlated to BWT than to MAAT. However, the relationship of brGMGTI with BWT ($r^2 = 0.91$) is similar to that with MAAT ($r^2 = 0.94$; Baxter et al., 2019; Russell et al., 2018), possibly owing in part to the sporadic nature of water measurements in these lakes but more fundamentally because the difference between BWT and local MAAT is generally small.

Moving away from the equator towards sub-tropical and warm-temperate regions, where seasonality in solar insolation (and hence, air temperature) increases, the difference between a stratifying lake's BWT (still similar to the annually lowest temperature of the daily mixed layer) and local MAAT becomes substantial, and then brGMGT-inferred temperature can be speculated to develop a bias towards the local cold-season air temperature. Finally, in cold-temperate regions where the BWT of stratifying lakes stabilizes at the temperature of greatest density (4 °C), brGMGTs may lose their usefulness as paleotemperature proxy.

Investigations of brGMGTs in the sediments of higher-latitude lakes are needed to test the influence of a greater offset between BWT and MAAT on brGMGT-based air-temperature calibrations. In addition, although soil-derived brGMGTs do not seem to contribute to the pool of brGMGTs found in Lake Chala, the relatively small size of the lake's catchment area and aerated conditions in its soils is not comparable to all lakes globally. In lakes where anoxia in catchment soils is more widespread, for example in wetlands where brGMGTs do occur abundantly (Naafs et al., 2018), they could comprise a larger part of the brGDGT pool, and thus influence the relationship between brGMGT distribution and air or water temperature. Future research should also focus on identifying which anaerobic bacteria produce brGMGTs in natural settings and if variation in their distribution is the result of shifts in microbial community composition or of a single group of bacteria modifying the structure of their lipid membrane. Although the association of specific isomers (both of brGMGTs and brGDGTs) with different temperature regimes may perhaps be more easily explained by shifts in active microbial communities, the strong theoretical link between the H-shaped structure and increased membrane stability at high temperatures prompts further investigation.

5. CONCLUSION

BrGMGTs in the water column of Lake Chala are mainly produced *in situ*, and predominantly in the anoxic zone. Their distribution and their abundance relative to the brGDGTs (%brGMGT) do not appear to be influenced by ambient water temperature or air temperature. The greatest production and diversity of brGMGTs occurs in the similarly anoxic surficial bottom sediments, and although it is unknown if this is true for all lakes, this may have consequences for the application of brGMGT-

based temperature models outside of the global tropics because of the greater difference, at least in stratifying lakes, between lake bottom-water temperature and local mean annual air temperature. BrGMGT-inferred MAAT estimates for Lake Chala are consistent with the model calibration based on East African lakes, supporting use of brGMGT-based proxies to reconstruct past temperature changes in East Africa from the sediment record of Lake Chala. More research is needed to determine which species of anaerobic bacteria produce the seven known brGMGTs and particularly to document where and when production occurs in stratifying non-tropical lakes. On the other hand, the more singular bottom-sediment source of lacustrine brGMGTs, as opposed to the mixed aquatic-terrestrial source of lacustrine brGDGTs, may confer greater reliability to brGMGT-based temperature reconstructions.

Declaration of Competing Interest

The authors declare that they have no known competing financial interests or personal relationships that could have appeared to influence the work reported in this paper.

ACKNOWLEDGEMENTS

We thank C. M. Oluseno for conducting the monthly lake sampling and monitoring, and A. Negash and P. de Regt for lipid extractions. We are grateful to L. van Bree for lipid extractions, sample analysis, discussions and help with creating plots. We further thank K. Nierop and D. Eefting at Utrecht University for lab assistance. Fieldwork with collection of the studied materials was carried out with permission from the government of Kenya through permit 13/001/11C to D.V. This research was supported by NESSC Gravitation Grant 024.002.001 from the Dutch Ministry of Education, Culture and Science (OCW) to J. S.S.D. The editor and three anonymous reviewers are thanked for their constructive comments that helped improve the manuscript.

RESEARCH DATA

Data from this paper are available in the Pangaea database (doi: 10.1594/PANGAEA.926916).

APPENDIX A. SUPPLEMENTARY MATERIAL

Supplementary data to this article can be found online at https://doi.org/10.1016/j.gca.2021.05.015.

REFERENCES

Barker P. A., Hurrell E. R., Leng M. J., Plessen B., Wolff C., Conley D. J., Keppens E., Milne I., Cumming B. F., Laird K. R., Kendrick C. P., Wynn P. M. and Verschuren D. (2013) Carbon cycling within an East African lake revealed by the carbon isotope composition of diatom silica: a 25-ka record from Lake Challa, Mt. Kilimanjaro. *Quat. Sci. Rev.* **66**, 55–63.

Bauersachs T. and Schwark L. (2016) Glycerol monoalkanediol diethers: A novel series of archaeal lipids detected in hydrothermal environments. *Rapid Commun. Mass Spectrom.* **30**, 54–60.

Baxter A. J., Hopmans E. C., Russell J. M. and Sinninghe Damsté J. S. (2019) Bacterial GMGTs in East African lake sediments: Their potential as palaeotemperature indicators. *Geochim. Cosmochim. Acta* **259**, 155–169.

Blaga C. I., Reichart G. J., Heiri O. and Sinninghe Damsté J. S. (2009) Tetraether membrane lipid distributions in water-column particulate matter and sediments: a study of 47 European lakes along a north–south transect. *J. Paleolimnol.* **41**, 523–540.

Blaauw M., van Geel B., Kristen I., Plessen B., Lyaruu A., Engstrom D. R., van der Plicht J. and Verschuren D. (2011) High-resolution ^{14}C dating of a 25,000 year lake-sediment record from equatorial East Africa. *Quat. Sci. Rev.* **30**, 3043–3059.

Bligh E. G. and Dyer W. J. (1959) A rapid method of total lipid extraction and purification. *Can. J. Biochem.* **37**, 911–917.

Bodé S., De Wispelaere L., Hemp A., Verschuren D. and Boeckx P. (2020) Water-isotope ecohydrology on Mt. Kilimanjaro. *Ecohydrol.* **13** e2171.

Berke M. A. (2018) Reconstructing terrestrial paleoenvironments using sedimentary organic biomarkers. In *Methods in Paleoecology*. Springer, Cham., pp. 121–149.

Bechtel A., Smittenberg R. H., Bernasconi S. M. and Schubert C. J. (2010) Distribution of branched and isoprenoid tetraether lipids in an oligotrophic and a eutrophic Swiss lake: insights into sources and GDGT-based proxies. *Org. Geochem.* **41**, 822–832.

van Bree L. G. J., Peterse F., van der Meer M. T. J., Middelburg J. J., Negash A. M. D., De Crop W., Cocquyt C., Wieringa J. J., Verschuren D. and Sinninghe Damsté J. S. (2018) Seasonal variability in the abundance and stable carbon-isotopic composition of lipid biomarkers in suspended particulate matter from a stratified equatorial lake (Lake Chala, Kenya/Tanzania): Implications for the sedimentary record. *Quat. Sci. Rev.* **192**, 208–224.

van Bree L. G. J., Peterse F., Baxter A. J., De Crop W., van Grinsven S., Villanueva L., Verschuren D. and Sinninghe Damsté J. S. (2020) Seasonal variability of in situ brGDGT production in a permanently stratified African crater lake. *Biogeosciences* **17**, 5443–5463.

Buckles L. K., Weijers J. W. H., Verschuren D. and Sinninghe Damsté J. S. (2014) Sources of core and intact branched tetraether membrane lipids in the lacustrine environment: Anatomy of Lake Challa and its catchment, equatorial East Africa. *Geochim. Cosmochim. Acta* **140**, 106–126.

Buckles L. K., Verschuren D., Weijers J. W. H., Cocquyt C., Blaauw M., Damsté J. and Sinninghe S. (2016) Interannual and (multi-) decadal variability in the sedimentary BIT index of Lake Challa, East Africa, over the past 2200 years: assessment of the precipitation proxy. *Clim. Past* **12**, 1243–1262.

Buckles L. K., Villanueva L., Weijers J. W. H., Verschuren D., Damsté J. and Sinninghe S. (2013) Linking isoprenoidal GDGT membrane-lipid distributions with gene abundances of ammonia-oxidising Thaumarchaeota and uncultured crenarchaeotal groups in the water column of a tropical lake (Lake Challa, East Africa). *Environ. Microbiol.* **15**, 2445–2462.

Castañeda I. S., Schefuß E., Pätzold J., Sinninghe Damsté J. S., Weldeab S. and Schouten S. (2010) Millennial-scale sea surface temperature changes in the eastern Mediterranean (Nile River

Delta region) over the last 27,000 years. *Paleoceanography* **25**, PA1208.

Castañeda I. S. and Schouten S. (2011) A review of molecular organic proxies for examining modern and ancient lacustrine environments. *Quat. Sci. Rev.* **30**, 2851–2891.

Chen Y., Zheng F., Chen S., Liu H., Phelps T. J. and Zhang C. (2018) Branched GDGT production at elevated temperatures in anaerobic soil microcosm incubations. *Org. Geochem.* **117**, 12–21.

Cohen A. S. (2003) *Paleolimnology: the history and evolution of lake systems*. Oxford University Press.

Colcord D. E., Pearson A. and Brassell S. C. (2017) Carbon isotopic composition of intact branched GDGT core lipids in Greenland lake sediments and soils. *Org. Geochem.* **110**, 25–32.

Dearing Crampton-Flood E., Tierney J. E., Peterse F., Kirkels F. M., Damsté J. and Sinninghe S. (2020) BayMBT: A Bayesian calibration model for branched glycerol dialkyl glycerol tetraethers in soils and peats. *Geochim. Cosmochim. Acta* **268**, 142–159.

De Crop W. and Verschuren D. (2019) Determining patterns of stratification and mixing in tropical crater lakes through intermittent water-column profiling: A case study in western Uganda. *J. African Earth Sci.* **153**, 17–30.

De Jonge C., Hopmans E. C., Stadnitskaia A., Rijpstra W. I. C., Hofland R., Tegelaar E., Damsté J. and Sinninghe S. (2013) Identification of novel penta-and hexamethylated branched glycerol dialkyl glycerol tetraethers in peat using HPLC–MS^2, GC–MS and GC–SMB-MS. *Org. Geochem.* **54**, 78–82.

De Jonge C., Hopmans E. C., Zell C. I., Kim J. H., Schouten S., Damsté J. and Sinninghe S. (2014) Occurrence and abundance of 6-methyl branched glycerol dialkyl glycerol tetraethers in soils: Implications for palaeoclimate reconstruction. *Geochim. Cosmochim. Acta* **141**, 97–112.

De Jonge C., Radujkovic D., Sigurdsson B. D., Weedon J. T., Janssens I. and Peterse F. (2019) Lipid biomarker temperature proxy responds to abrupt shift in the bacterial community composition in geothermally heated soils. *Org. Geochem.* **137** 103897.

Dos Santos R. A. L., Prange M., Castañeda I. S., Schefuß E., Mulitza S., Schulz M., Niedermeyer E. M., Sinninghe Damsté J. S. and Schouten S. (2010) Glacial–interglacial variability in Atlantic meridional overturning circulation and thermocline adjustments in the tropical North Atlantic. *Earth Planet. Sci. Lett.* **300**, 407–414.

Eickmann B., Baumberger T., Thorseth I. H., Strauss H., Früh-Green G. L., Pedersen R. B. and Jaeschke A. (2020) Subseafloor sulfur cycling in a low-temperature barite field: A multi-proxy study from the Arctic Loki's Castle vent field. *Chem. Geol.* **539** 119495.

Hemp A. (2006) Continuum or zonation? Altitudinal gradients in the forest vegetation of Mt. Kilimanjaro. *Plant Ecol.* **184**, 27–42.

Hopmans E. C., Schouten S., Damsté J. and Sinninghe S. (2016) The effect of improved chromatography on GDGT-based palaeoproxies. *Org. Geochem.* **93**, 1–6.

Huguet C., Hopmans E. C., Febo-Ayala W., Thompson D. H., Sinninghe Damsté J. S. and Schouten S. (2006) An improved method to determine the absolute abundance of glycerol dibiphytanyl glycerol tetraether lipids. *Org. Geochem.* **37**, 1036–1041.

Jaeschke A., Jørgensen S., Bernasconi S., Pederse R., Thorseth I. and Früh-Green G. (2012) Microbial diversity of Loki's Castle black smokers at the Arctic Mid-Ocean Ridge. *Geobiology* **10**, 548–561.

Jia C., Zhang C. L., Xie W., Wang J. X., Li F., Wang S., Dong H., Li W. and Boyd E. S. (2014) Differential temperature and pH controls on the abundance and composition of H-GDGTs in terrestrial hot springs. *Org. Geochem.* **75**, 109–121.

Johnson T. C., Werne J. P., Brown E. T., Abbott A., Berke M., Steinman B. A., Halbur J., Contreras S., Grosshuesch S., Deino A. and Scholz C. A. (2016) A progressively wetter climate in southern East Africa over the past 1.3 million years. *Nature* **537**, 220–224.

Kim J. H., Van der Meer J., Schouten S., Helmke P., Willmott V., Sangiorgi F., Koç N., Hopmans E. C., Damsté J. and Sinninghe S. (2010) New indices and calibrations derived from the distribution of crenarchaeal isoprenoid tetraether lipids: Implications for past sea surface temperature reconstructions. *Geochim. Cosmochim. Acta* **74**, 4639–4654.

Kirkels F. M. S. A., Ponton C., Galy V., West A. J., Feakins S. J. and Peterse F. (2020) From Andes to Amazon: assessing branched tetraether lipids as tracers for soil organic carbon in the madre de dios river system. *J. Geophys. Res. Biogeochem.* **125**, e2019JG005270.

Knappy C. S., Nunn C. E., Morgan H. W. and Keely B. J. (2011) The major lipid cores of the archaeon *Ignisphaera aggregans*: implications for the phylogeny and biosynthesis of glycerol monoalkyl glycerol tetraether isoprenoid lipids. *Extremophiles* **15**, 517.

Lê S., Josse J. and Husson F. (2008) FactoMineR: An R Package for Multivariate Analysis. *J. Stat. Softw.* **25**, 1–18.

Lewis W. M. (1983) A revised classification of lakes based on mixing. *Can. J. Fish. Aquat. Sci.* **40**, 1779–1787.

Lewis W. M. (1987) Tropical limnology. *Annu. Rev. Ecol. Syst.* **18**, 159–184.

Liu X. L., Summons R. and Hinrichs K. U. (2012) Extending the known range of glycerol ether lipids in the environment: Structural assignments based on tandem mass spectral fragmentation patterns. *Rapid Commun. Mass Spectrom.* **26**, 2295–2302.

Loomis S. E., Russell J. M., Damsté J. and Sinninghe S. (2011) Distributions of branched GDGTs in soils and lake sediments from western Uganda: implications for a lacustrine paleothermometer. *Org. Geochem.* **42**, 739–751.

Loomis S. E., Russell J. M., Ladd B., Street-Perrott F. A., Damsté J. and Sinninghe S. (2012) Calibration and application of the branched GDGT temperature proxy on East African lake sediments. *Earth Planet. Sci. Lett.* **357**, 277–288.

Loomis S. E., Russell J. M., Eggermont H., Verschuren D., Damsté J. and Sinninghe S. (2014) Effects of temperature, pH and nutrient concentration on branched GDGT distributions in East African lakes: Implications for paleoenvironmental reconstruction. *Org. Geochem.* **66**, 25–37.

Lutnaes B. F., Brandal Ø., Sjöblom J. and Krane J. (2006) Archaeal C 80 isoprenoid tetraacids responsible for naphthenate deposition in crude oil processing. *Org. Biomol. Chem.* **4**, 616–620.

Lutnaes B. F., Krane J., Smith B. E. and Rowland S. J. (2007) Structure elucidation of C 80, C 81 and C 82 isoprenoid tetraacids responsible for naphthenate deposition in crude oil production. *Org. Biomol. Chem.* **5**, 1873–1877.

Meyer I., Van Daele M., Tanghe N., De Batist M. and Verschuren D. (2020) Reconstructing East African monsoon variability from grain-size distributions: End-member modeling and source attribution of diatom-rich sediments from Lake Chala. *Quat. Sci. Rev.* **247** 106574.

Meyers P. A. (2003) Applications of Org. Geochem. to paleolimnological reconstructions: a summary of examples from the Laurentian Great Lakes. *Org. Geochem.* **34**, 261–289.

Miller D. R., Habicht M. H., Keisling B. A., Castañeda I. S. and Bradley R. S. (2018) A 900-year New England temperature reconstruction from in situ seasonally produced branched glycerol dialkyl glycerol tetraethers (brGDGTs). *Clim. Past* **14**, 1653–1667.

Moernaut J., Verschuren D., Charlet F., Kristen I., Fagot M. and De Batist M. (2010) The seismic-stratigraphic record of lake-level fluctuations in Lake Challa: Hydrological stability and change in equatorial East Africa over the last 140 kyr. *EPSL* **290**, 214–223.

Morii H., Eguchi T., Nishihara M., Kakinuma K., Konig H. and Kogaa Y. (1998) A novel ether core lipid with H-shaped C-80-isoprenoid hydrocarbon chain from the hyperthermophilic methanogen *Methanothermus fervidus*. *Bioch. Biophys. Acta - Lipids Lipid Metabol.* **1390**, 339–345.

Naafs B. D. A., Gallego-Sala A. V., Inglis G. N. and Pancost R. D. (2017a) Refining the global branched glycerol dialkyl glycerol tetraether (brGDGT) soil temperature calibration. *Org. Geochem.* **106**, 48–56.

Naafs B. D. A., Inglis G. N., Zheng Y., Amesbury M. J., Biester H., Bindler R., Blewett J., Burrows M. A., Del Castillo Torres D., Chambers F. M. and Cohen A. D. (2017b) Introducing global peat-specific temperature and pH calibrations based on brGDGT bacterial lipids. *Geochim. Cosmochim. Acta* **208**, 285–301.

Naafs B. D. A., McCormick D., Inglis G. N. and Pancost R. D. (2018) Archaeal and bacterial H-GDGTs are abundant in peat and their relative abundance is positively correlated with temperature. *Geochim. Cosmochim. Acta* **227**, 156–170.

Pan A., Yang Q., Zhou H., Ji F., Wang H. and Pancost R. D. (2016) A diagnostic GDGT signature for the impact of hydrothermal activity on surface deposits at the Southwest Indian Ridge. *Org. Geochem.* **99**, 90–101.

Payne B. R. (1970) Water balance of Lake Chala and its relation to groundwater from tritium and stable isotope data. *J. Hydrol.* **11**, 47–58.

Pearson E. J., Juggins S., Talbot H. M., Weckström J., Rosén P., Ryves D. B., Roberts S. J. and Schmidt R. (2011) A lacustrine GDGT-temperature calibration from the Scandinavian Arctic to Antarctic: Renewed potential for the application of GDGT-paleothermometry in lakes. *Geochim. Cosmochim. Acta* **75**, 6225–6238.

Powers L. A., Werne J. P., Johnson T. C., Hopmans E. C., Sinninghe Damsté J. S. and Schouten S. (2004) Crenarchaeotal membrane lipids in lake sediments: a new paleotemperature proxy for continental paleoclimate reconstruction? *Geology* **32**, 613–616.

Russell J. M., Hopmans E. C., Loomis S. E., Liang J., Damsté J. and Sinninghe S. (2018) Distributions of 5- and 6-methyl branched glycerol dialkyl glycerol tetraethers (brGDGTs) in East African lake sediment: Effects of temperature, pH, and new lacustrine paleotemperature calibrations. *Org. Geochem.* **117**, 56–69.

Schouten S., Hopmans E. C., Schefuß E. and Sinninghe Damsté J. S. (2002) Distributional variations in marine crenarchaeotal membrane lipids: A new tool for reconstructing ancient sea water temperatures? *Earth Planet Sci. Lett.* **204**, 265–274.

Schouten S., Baas M., Hopmans E. C., Reysenbach A. L. and Sinninghe Damsté J. S. (2008a) Tetraether membrane lipids of *Candidatus* "Aciduliprofundum boonei", a cultivated obligate thermoacidophilic euryarchaeote from deep-sea hydrothermal vents. *Extremophiles* **12**, 119–124.

Schouten S., Baas M., Hopmans E. C., Damsté J. and Sinninghe S. (2008b) An unusual isoprenoid tetraether lipid in marine and lacustrine sediments. *Org. Geochem.* **39**, 1033–1038.

Schouten S., Hopmans E. C., Damsté J. and Sinninghe S. (2013) The organic geochemistry of glycerol dialkyl glycerol tetraether lipids: A review. *Org. Geochem.* **54**, 19–61.

Shanahan T. M., Hughen K. A. and Van Mooy B. A. S. (2013) Temperature sensitivity of branched and isoprenoid GDGTs in Arctic lakes. *Org. Geochem.* **64**, 119–128.

Sinninghe Damsté J. S., Hopmans E. C., Pancost R. D., Schouten S. and Geenevasen J. A. (2000) Newly discovered non-isoprenoid glycerol dialkyl glycerol tetraether lipids in sediments. *Chem. Comm.* **17**, 1683–1684.

Sinninghe Damsté J. S., Ossebaar J., Abbas B., Schouten S. and Verschuren D. (2009) Fluxes and distribution of tetraether lipids in an equatorial African lake: constraints on the application of the TEX86 palaeothermometer and BIT index in lacustrine settings. *Geochim. Cosmochim. Acta* **73**, 4232–4249.

Sinninghe Damsté J. S., Rijpstra W. I. C., Hopmans E. C., Weijers J. W., Foesel B. U., Overmann J. and Dedysh S. N. (2011) 13,16-Dimethyl octacosanedioic acid (iso-diabolic acid), a common membrane-spanning lipid of Acidobacteria subdivisions 1 and 3. *Appl. Environm. Microbiol.* **77**, 4147–4154.

Sinninghe Damsté J. S., Rijpstra W. I. C., Hopmans E. C., Foesel B. U., Wüst P. K., Overmann J., Tank M., Bryant D. A., Dunfield P. F., Houghton K. and Stott M. B. (2014) Ether-and ester-bound iso-diabolic acid and other lipids in members of acidobacteria subdivision 4. *Appl. Environm. Microbiol.* **80**, 5207–5218.

Sinninghe Damsté J. S., Rijpstra W. I. C., Foesel B. U., Huber K. J., Overmann J., Nakagawa S., Kim J. J., Dunfield P. F., Dedysh S. N. and Villanueva L. (2018) An overview of the occurrence of ether- and ester-linked iso-diabolic acid membrane lipids in microbial cultures of the Acidobacteria: Implications for brGDGT paleoproxies for temperature and pH. *Org. Geochem.* **124**, 63–76.

Sluijs A., Schouten S., Pagani M., Woltering M., Brinkhuis H., Sinninghe Damsté J. S., Dickens G. R., Huber M., Reichart G. J., Stein R. and Matthiessen J. (2006) Subtropical Arctic Ocean temperatures during the Palaeocene/Eocene thermal maximum. *Nature* **44**, 610–613.

Sluijs A., Frieling J., Inglis G. N., Nierop K. G., Peterse F., Sangiorgi F. and Schouten S. (2020) Late Paleocene–early Eocene Arctic Ocean Sea Surface Temperatures; reassessing biomarker paleothermometry at Lomonosov Ridge. *Clim. Past.* **16**, 2381–2400.

Sollich M., Yoshinaga M. Y., Häusler S., Price R. E., Hinrichs K. U. and Bühring S. I. (2017) Heat stress dictates microbial lipid composition along a thermal gradient in marine sediments. *Front. Microbiol.* **8**, 1550.

Talling J. F. (1969) The incidence of vertical mixing, and some biological and chemical consequences, in tropical African lakes. *Verh. Internat. Verein. Theor. Angew. Limnol.* **17**, 998–1012.

Tang X., Naafs B. D., Pancost R. D., Liu Z., Fan T. and Zheng Y. (2021) Exploring the influences of temperature on "H-Shaped" Glycerol Dialkyl Glycerol Tetraethers in a stratigraphic context: evidence from two peat cores across the late Quaternary. *Front. Earth Sci.* **8** 541685.

Tierney J. E. and Russell J. M. (2009) Distributions of branched GDGTs in a tropical lake system: implications for lacustrine application of the MBT/CBT paleoproxy. *Org. Geochem.* **40**, 1032–1036.

Tierney J. E., Russell J. M., Eggermont H., Hopmans E. C., Verschuren D., Damsté J. and Sinninghe S. (2010) Environmental controls on branched tetraether lipid distributions in tropical East African lake sediments. *Geochim. Cosmochim. Acta* **74**, 4902–4918.

Verschuren D., Olago D. O., Rucina S. M. and Odhengo P. O. (2013) DeepCHALLA: two glacial cycles of climate and ecosystem dynamics from equatorial East Africa. *Scientific Drilling* **15**, 72–75.

Verschuren D., Sinninghe Damsté J. S., Moernaut J., Kristen I., Blaauw M., Fagot M., Haug G.H. and CHALLACEA Project Members (2009) Half-precessional dynamics of monsoon rainfall near the East African Equator. Nature 462, 637–641.

Verburg P. and Hecky R. E. (2009) The physics of the warming of Lake Tanganyika by climate change. *Limnol. Oceanogr.* **54**, 2418–2430.

Wolff C., Haug G. H., Timmermann A., Sinninghe Damsté J. S., Brauer A., Sigman D. M., Cane M. A. and Verschuren D. (2011) Reduced interannual rainfall variability in East Africa during the last ice age. *Science* **333**, 743–747.

Wolff C., Kristen-Jenny I., Schettler G., Plessen B., Meyer H., Dulski P., Naumann R., Brauer A., Verschuren D. and Haug G. H. (2014) Modern seasonality in Lake Challa (Kenya/Tanzania) and its sedimentary documentation in recent lake sediments. *Limnol. Oceanogr.* **59**, 1621–1636.

Weber Y., De Jonge C., Rijpstra W. I. C., Hopmans E. C., Stadnitskaia A., Schubert C. J., Lehmann M. F., Sinninghe Damsté J. S. and Niemann H. (2015) Identification and carbon isotope composition of a novel branched GDGT isomer in lake sediments: Evidence for lacustrine branched GDGT production. *Geochim. Cosmochim. Acta* **154**, 118–129.

Weber Y., Sinninghe Damsté J. S., Zopfi J., DeJonge C., Gilli A., Schubert C. J., Lepori F., Lehmann M. F. and Niemann H. (2018) Redox-dependent niche differentiation provides evidence for multiple bacterial sources of glycerol tetraether lipids in lakes. *Proc. Natl. Acad. Sci. U.S.A.* **115**, 10926–10931.

Weijers J. W. H., Schouten S., Hopmans E. C., Geenevasen J. A., David O. R., Coleman J. M., Pancost R. D., Damsté J. and Sinninghe S. (2006a) Membrane lipids of mesophilic anaerobic bacteria thriving in peats have typical archaeal traits. *Environ. Microbiol.* **8**, 648–657.

Weijers J. W. H., Schouten S., Spaargaren O. C., Damsté J. and Sinninghe S. (2006b) Occurrence and distribution of tetraether membrane lipids in soils: Implications for the use of the TEX_{86} proxy and the BIT index. *Org. Geochem.* **37**, 1680–1693.

Weijers J. W. H., Schouten S., van den Donker J. C., Hopmans E. C., Damsté J. and Sinninghe S. (2007) Environmental controls on bacterial tetraether membrane lipid distribution in soils. *Geochim. Cosmochim. Acta* **71**, 703–713.

Xie S., Liu X. L., Schubotz F., Wakeham S. G. and Hinrichs K. U. (2014) Distribution of glycerol ether lipids in the oxygen minimum zone of the Eastern Tropical North Pacific Ocean. *Org. Geochem.* **71**, 60–71.

Yang H., Xiao W., Słowakiewicz M., Ding W., Ayari A., Dang X. and Pei H. (2019) Depth-dependent variation of archaeal ether lipids along soil and peat profiles from southern China: Implications for the use of isoprenoidal GDGTs as environmental tracers. *Org. Geochem.* **128**, 42–56.

Associate editor: Shucheng Xie